Emeralds in Hiddenite, NC:
Using circular seismic arrays to identify gem-hosting quartz veins

Jessica Lindsay
April 25, 2019
GEOL394

Advisors: Dr. Nicholas Schmerr,
& Dr. Mong-han Huang

Abstract

Quartz veins in saprolite and bedrock near Hiddenite, North Carolina can contain cavities that may bear emeralds, in addition to other minerals. This means, in order to find the emeralds, one must find the veins. To avoid spending, time, money, and effort inefficiently, this project explored the use of circular, multi-channel seismic arrays to attempt to identify these veins without requiring previous excavation of overburden. The method is very similar to that of Novitsky et al. (2018), who found that linear subsurface features, like faults and fractures, produce identifiable patterns of anisotropy in saprolite. Using an active source, first arrival times of direct and refracted P-waves were found along 30° lines of azimuth on two circular arrays; one 15m in diameter, the other 12m. These first arrival times were then inverted using the Trans-dimensional Bayesian method, which outputs a large number of potential one-dimensional models by allowing velocities, depth, and number of layers to vary. High error limited the conclusions that can be drawn regarding where to dig for veins but allowed for the discovery of upper bounds on the amount of anisotropy present beneath these arrays.

Introduction

The town of Hiddenite in North Carolina is currently North America's most productive area for the mining of emeralds, producing the largest specimens in the United States. Despite being named for a chromium-bearing variety of spodumene, the town has been described as having "the most important emerald deposits in North America" (Sinkankas, 1989). Intermittent small-scale mining of the area has yielded numerous spectacular specimens of emerald since discovery in the mid-1870s, and the area continues to be of great interest to mineral enthusiasts, gemologists, and the scientific community.

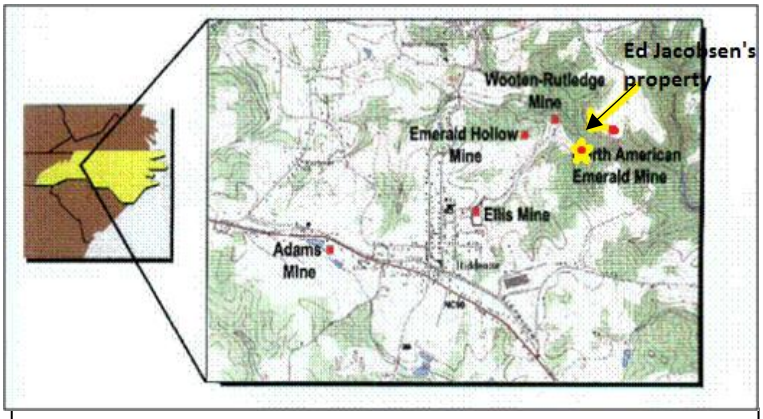

***Figure 1**: Showing relative position of Mr. Jacobsen's property to other mines in the immediate area. Adapted from Speer (2008).*

Emeralds are a colored variety of the mineral beryl ($Be_3Al_2(SiO_3)_6$), characterized by inclusions of chromium and/or vanadium that cause the crystals to reflect green light. Emerald has been considered a precious gemstone since before recorded history, usually for decorative value and the novelty of its green color (Sinkankas, 1989). The largest of the emeralds from Hiddenite was found at the North American Emerald Mine (NAEM) in 2003, weighing 1,869 carats (Speer, 2008).

Ed Jacobsen is an alumnus of the University of Maryland Geology Program. Drawn by the allure of emerald finds in the area over the past 150 years, Mr. Jacobsen purchased land 1 km northeast of downtown Hiddenite, intending to do some digging of his own. His land is 0.5 km southwest of NAEM (Figure 1). For the past several years, Mr. Jacobsen and his employees have been digging with a backhoe and a bulldozer. However, the saprolite is sticky and clay-rich; it holds moisture well and makes very difficult digging for human and backhoe alike. Because the saprolite is so effective at retaining moisture, it also prevents Ground Penetrating Radar (GPR) from penetrating more than a few feet beneath the surface. For this reason, GPR surveys of Mr. Jacobsen's property have been less than helpful in the search for gem-bearing veins. Some small emeralds have been discovered floating in the saprolite on the property, and veins containing quartz, feldspar, and rutile have also been excavated, but no gem-bearing pockets have been found to date. Currently, Mr. Jacobsen lacks effective, non-invasive methods of finding the veins which normally host the emeralds. If this project proves to be successful for the intended purpose, it can be considered a relatively simple and inexpensive means of identifying subsurface linear ore bodies without the prior removal of overburden. Traditional methods for locating subsurface ore bodies include drilling, gravity surveying, and GPR. However, specific and often-expensive pieces of equipment are required for drilling and gravity surveys, and GPR has already been disqualified because of the water-content of the saprolite. Tomography using crossing ray-paths is time-consuming and comparatively complicated. The goal of this project is to help Mr. Jacobsen find "minerals of economic value", using a method that requires less time and labor than blind digging.

Background Geology

Hiddenite is located in the intensely deformed and metamorphosed Inner Piedmont Belt of western North Carolina, a nearly 100 km wide area that extends approximately 700 km southwest of the Sauratown Mountain window in North Carolina to Alabama. The Inner Piedmont Belt is bounded on the east by the Carolina Piedmont Suture, separating it from the Carolina Terrane, and on the west side by the northeast-trending Brevard Fault Zone, separating it from the Blue Ridge (Wise, 2009) (Figure 2). The Inner Piedmont Belt is only one of many exotic terranes in this region and the constituent rocks have experienced multiple continental collision events (Rankin et al., 1989). Unfortunately, specific details of the geology in this region can be uncertain. The ages of the rocks are often not very constrained, and the lithology is complex enough to warrant use of the amusing term "megamelange" (Drake et al., 1989). Overall, the Inner Piedmont Belt consists of 500 to 750 Ma old sillimanite-grade rocks, including gneisses, migmatites, and schists that have been intruded by numerous deep- and shallow-level granitic to gabbroic plutons (see Figure 3, next page).

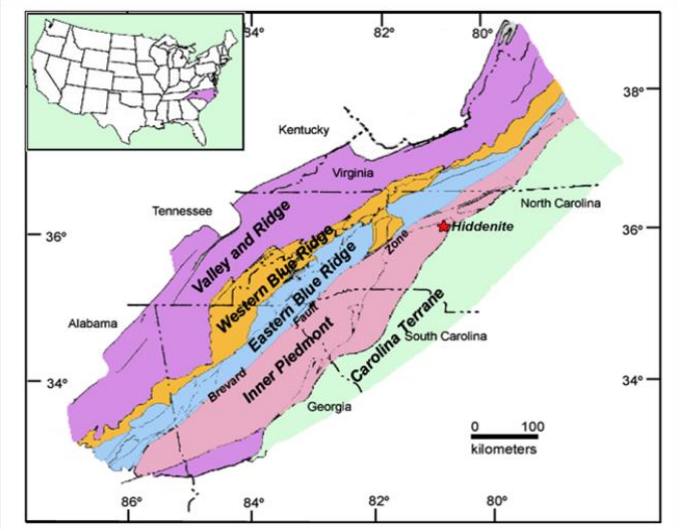

Figure 2: *General geological provinces of the southern Appalachians showing the location of Hiddenite, NC. From Wise (2009).*

The bedrock geology of the Hiddenite area consists of Precambrian migmatitic schists and gneisses that are cross-cut by an extensive set of steeply-dipping, north- to northeast-trending quartz veins (Figure 4, next page). Prolonged weathering of the migmatitic bedrock has resulted in the formation of a thick, red saprolite horizon (Wise & Anderson, 2006). Quartz veins may be identified near the surface in this saprolite and followed downward into the unweathered bedrock below.

Early details of the geology and mineralogy of the quartz veins in this area were provided by Palache et al. (1930) and Sinkankas (1976) and more recently by Wise and Anderson (2006) and Wise (2009). The origin of the quartz veins has previously been attributed to pegmatites (Palache et al., 1930; Brown & Wilson, 2001). However, Sinkankas (1976, 1989), Tacker (1999), and Wise and Anderson (2006) all advocate crystallization from hydrothermal fluids. The Hiddenite quartz veins show a remarkable similarity in their structure and mineral assemblage to "Alpine-type" veins: hydrothermal fluid deposits infilling brittle tension fractures that developed during regional deformation in the Swiss Alps (Sinkankas, 1976; Campbell, 1927).

The veins at Hiddenite are characterized by massive white quartz exhibiting a comb-texture, growing from the walls towards the center of pockets. Other minerals can be found in these pockets as well, either growing in a manner similar to the quartz, on the surfaces of other minerals, or as float, having been broken off the walls of the cavity. In addition to white quartz, observed minerals include amethystine quartz, mica, albite, apatite, rutile, dolomite, calcite, siderite, and pyrite. Emeralds, colorless beryl, hiddenite, apatite, monazite, and molybdenite can occur as accessory minerals. Xenotime, tourmaline, garnet, nontronite, and arsenopyrite have also been reported in veins from this area (Sinkankas, 1989) but have not been personally observed.

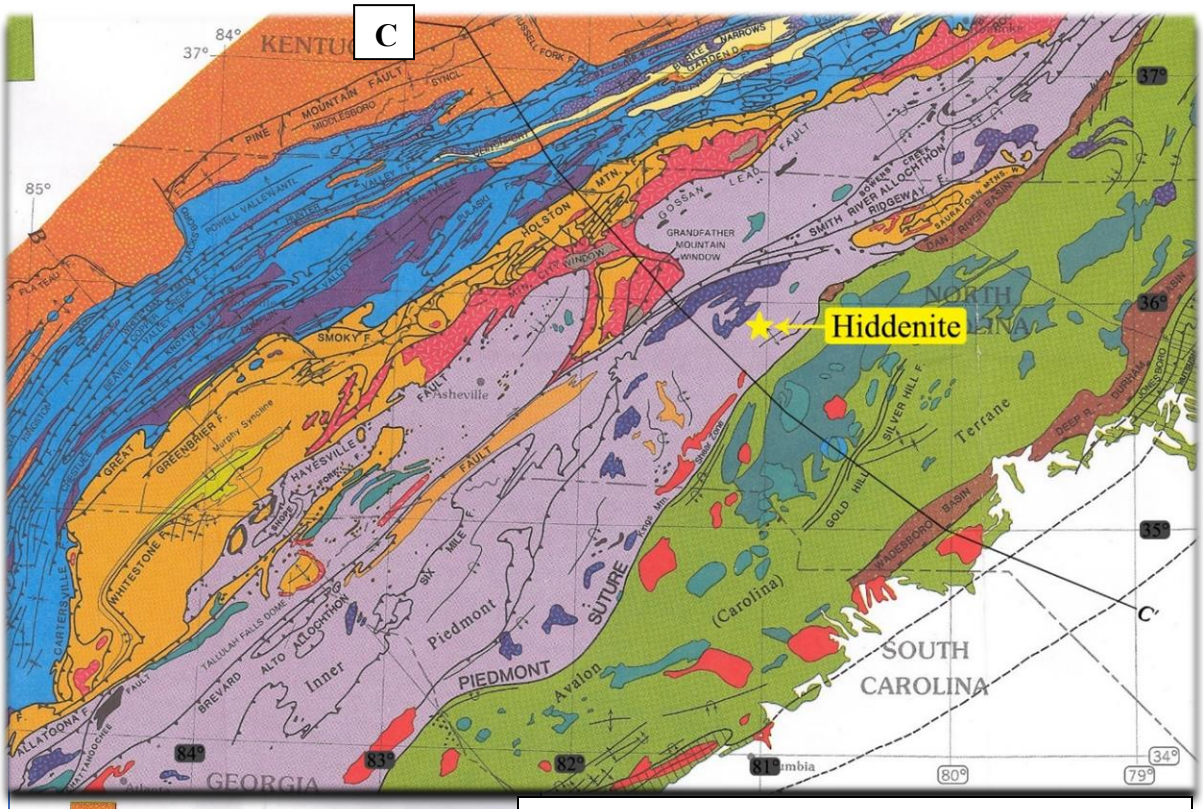

Late Mississippian-Permian molasse and Middle Devonian-Permian molasse (New England) Carboniferous-Permian intrusions.

North American Paleozoic platform / Taconian clastic wedge (Upper Ordovician-Silurian Martinsburg-Shawangunk patterned) / Acadian clastic wedge

Late Proterozoic and Cambrian clastic deposits of the North American continental margin / Late Proterozoic-Ordovician outer margin deposits of the Taconic allochthons and Hamburg klippe.

North American basement massifs / Late Proterozoic alkalic plutons, Southern Appalachians/ Chain Lakes massif/ Chain Lakes pre-Arenigian cover.

Alleghanian metamorphic overprint (approx; extent).

Ultramafic rocks (includes mafic-Ultramafic complexes)

North American outer margin cover sequence including late Proterozoic-Ordovician accretionary prisms / Cambrian-Middle Ordovician Intrusions.

Cambrian-Ordovician cover (including Ordovician arc volcanic rocks of medial New England) Late Proterozoic-Ordovician tonalitic gneisses amphibolites and granitoid intrusions. Includes Penobscottian (?) intrusions in entire orogen / basement of medial New England.

Silurian-Early Devonian cover of medial New England / Ordovician-Silurian-Devonian deep-water facies of Talladega and Murphy belts / Acadian (Late Ordovician through Devonian) intrusions.

Late Proterozoic-Cambrian sedimentary and volcanic rocks of Avalon / Late Proterozoic sedimentary and volcanic rocks of Avalon (basement?) / sequences belonging either to avalon or medial New England / Late Proterozoic-Cambrian intrusions.

Silurian to Early Devonian cover of Avalon (New England) / Ordovician and Devonian alkalic intrusions and associated volcanic rocks of Avalon.

Figure 3 *– Top: Geological map of region, showing approximate location of Hiddenite, NC. Left: Legend. Next page: Geological cross section of C-C'. Adapted from Hatcher et al. (1990).*

Figure 4: *System of quartz veins in bedrock at NAEM. Photo courtesy of Dr. Michael Wise.*

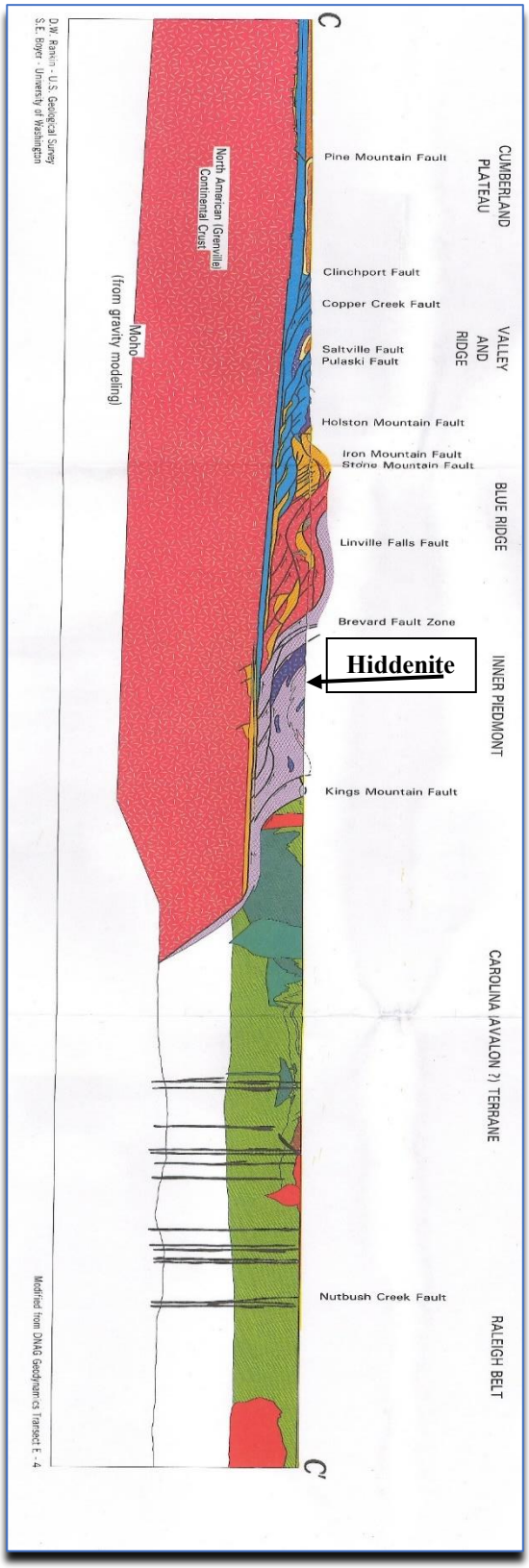

Hypotheses

The premise for this project is based on a study by Novitsky et al. (2018), who found, using circular seismic arrays that P-wave velocities were highest along the strike of steeply-dipping features, like faults and fractures in saprolite and schistose materials like those present at Hiddenite (Figure 5). The steeply-dipping quartz veins at Hiddenite are the result of fractures, and they are made of harder material than the weathered saprolite they inhabit. Not only that, but there does appear to be a directional control on the orientation of these veins. Recall that the majority of veins at NAEM are north- to northeast-trending. In light of these observations, our hypotheses comment on possible relationships between anisotropy and the position of quartz veins on Mr. Jacobsen's property. The hypotheses evaluated as part of this work are as follows:

I. Local orientation of the country rock will produce seismic anisotropy with the same orientation as regional trends.

II. Local anisotropy is controlled by the presence of mineralized veins.

NULL: Local anisotropy is controlled neither by regional trends nor the presence of veins.

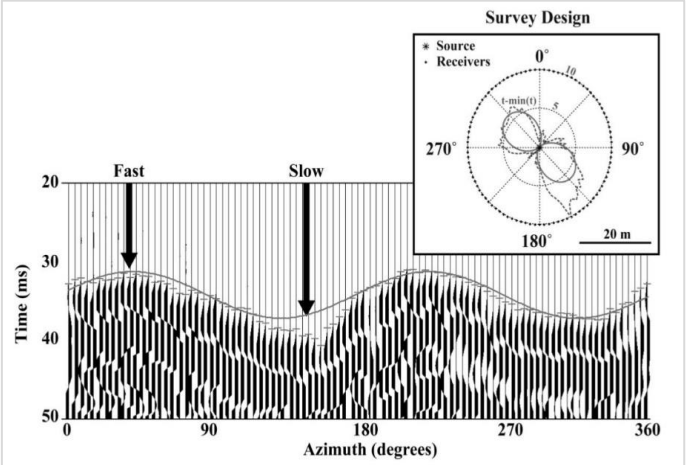

Figure 5: *Arrival times of waves using a circular array method plotted against azimuthal direction. From Novitsky et al. (2018), who found that the fast directions occurred along strike of linear features in saprolite and schistose materials.*

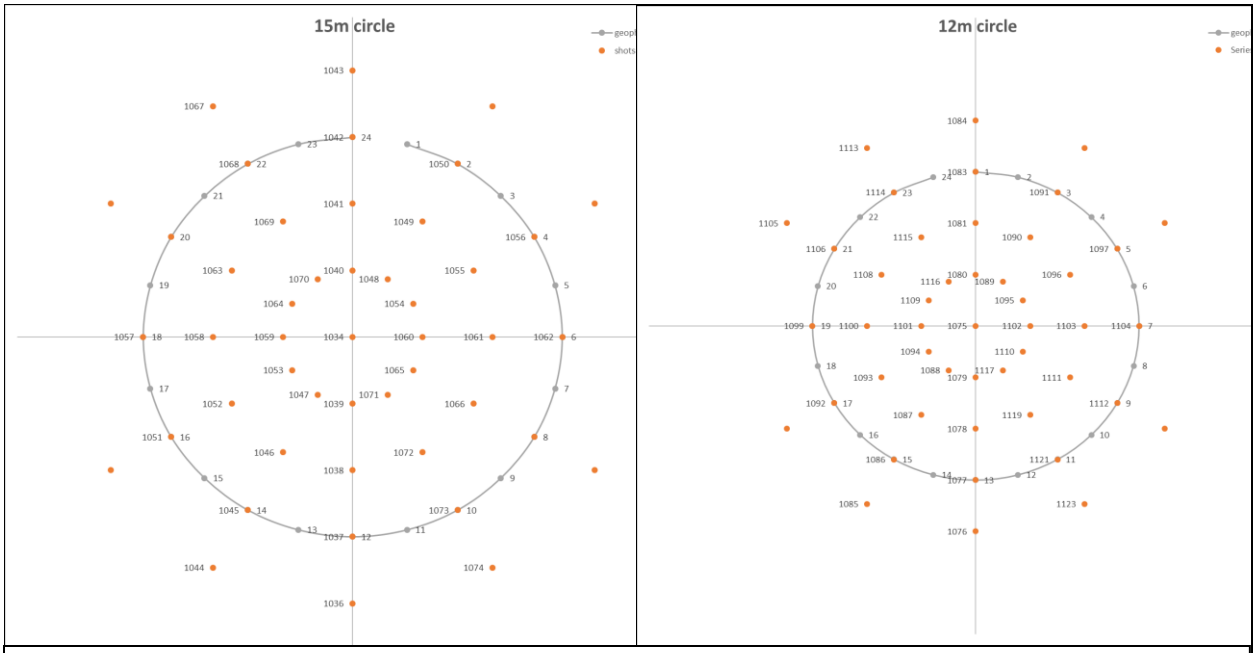

Figure 6: *Relative positions of shots and geophones for each array. Geophones (1-24) are grey dots on perimeter of circle. Shots are orange; four-digit numbers associated with each is a reference number. Un-numbered dots are shots that were impossible due to topography. Where shots and geophones overlap, the first arrival time at that geophone was declared to be 0ms. The distance between shots on each line of azimuth for the 15m array was 2m. This distance was 1.5 m for the 12m array. Sampled lines of azimuth are in increments of 30° clockwise from North (00°).*

Methods

The construction of a circular seismic array is straight-forward, and an array can be placed on saprolite or bedrock. Each array has 24 14-Hz vertical-component geophones placed at regular intervals on the perimeter of a circle. A 30x30 cm steel plate was struck with an 8kg hammer to produce vibrations at specific positions within and without the circle (Figure 6), and the geophones record the arrival time of those waves. The geophones and a piezoelectric sensor on the hammer are connected to an ES3000 Multichannel Seismic Recorder (produced by Geometrics). When the hammer contacts the metal plate, the sensor triggers the system to start recording and automatically stop after one second with a sample rate of 16 kHz**.** After each shot, preliminary readings were observed on a field laptop and evaluated for quality. If the sledgehammer bounced twice, any bystander moved during the shot, or any other factor may have influenced the reading, the data from that shot was discarded and another was performed to replace it. There was no stacking, in the interest of time. There were over one hundred shots performed over the course of the day.

Locations for the arrays were selected based on available space and an outcropping of vein material at the surface (Figure 7). At the first location, the array had a diameter of 15 m. The ground here was almost entirely cleared of trees and debris, which allowed for the larger diameter. The array at the second location had a diameter of 12 m and a vein outcropping in the northwestern quadrant. The presence of this vein material should act as a control; it is a known entity. This second site was also in an area where a significant volume of material had been excavated from a slope. Consequently, the size of the array was limited by the dimensions of this excavation.

In the interest of time, shots were performed at regular intervals along five lines of azimuth for each array: 00° (north-south), 30°, 60°, 90°, 120°, and 150°. Even if a vein were to occur precisely between these lines of azimuth, there should be still be an observable difference

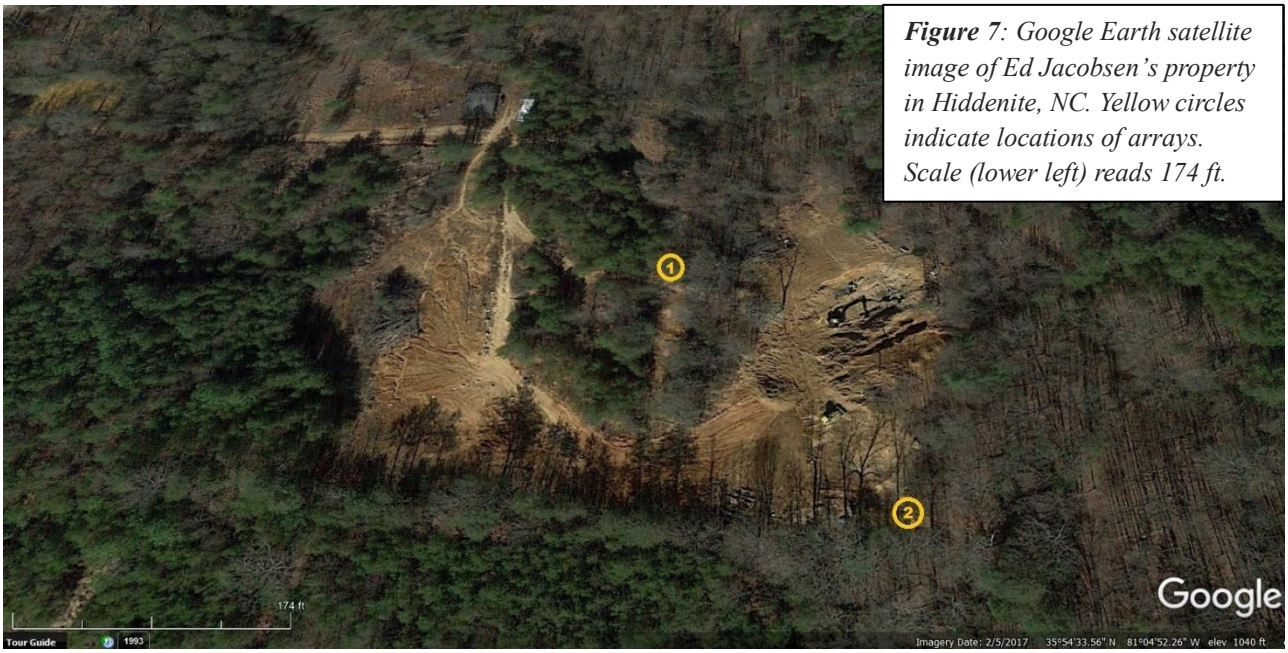

***Figure 7**: Google Earth satellite image of Ed Jacobsen's property in Hiddenite, NC. Yellow circles indicate locations of arrays. Scale (lower left) reads 174 ft.*

in velocity between the adjacent lines of azimuth and those lines perpendicular to them. If Novitsky et al.'s findings can be applied here, then the slow direction should be perpendicular to any veins. The difference in velocity would still be measurable, even if veins do not occur precisely along a sampled line of azimuth. After analysis, directions identified as being fast or slow can then be compared to local and regional trends (like the strike of the Appalachian Mountains) to test the hypotheses.

Data Analysis

More than one hundred shots performed yielded more than a hundred seismograms from which to pick first arrival times of the P-waves. A picking program, Pickwin, was used for this purpose. The first breaks were manually selected as the first deviation from zero ahead of significant peaks, for the sake of consistency (Figure 8). The picking error was less than 0.5 ms, determined by the size of the mouse cursor on the computer screen.

After picking the first breaks for each seismograph, Pickwin returns a text file with geophone number and the picked arrival time for each shot (Figure 8). This data can then be put into a table to create time-travel curves for each 30° line of azimuth. In order to create a model of the nature of the subsurface, it is necessary to find a best-fit line for this time-travel curve. This best-fit line represents the velocity of the waves within the subsurface material. A line of constant slope indicates a single velocity throughout the material, while a line with multiple slopes represents velocity changes which may be correlated with a change of material consistency, or even layer contacts (Burger et al., 2006)

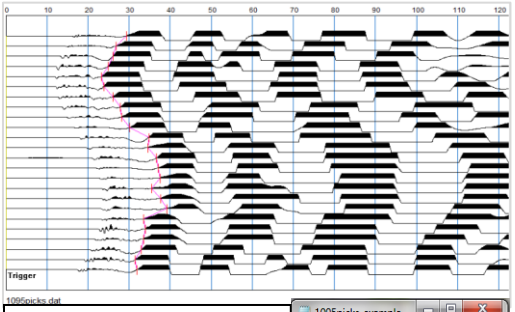

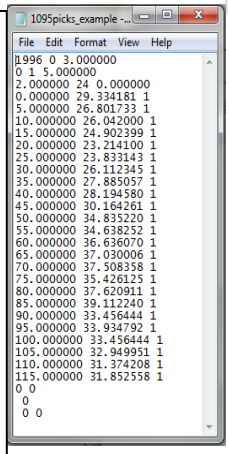

***Figure 8**: Top: Example of a returned seismogram for shot #1095. X-axis is Time (ms), and y-axis is Geophone position (1-24). Red line indicates picked positions of first breaks.*
Right: Format of text file, returned by Pickwin after picking first breaks. First column indicates geophone position and second column is picked arrival time (in ms).

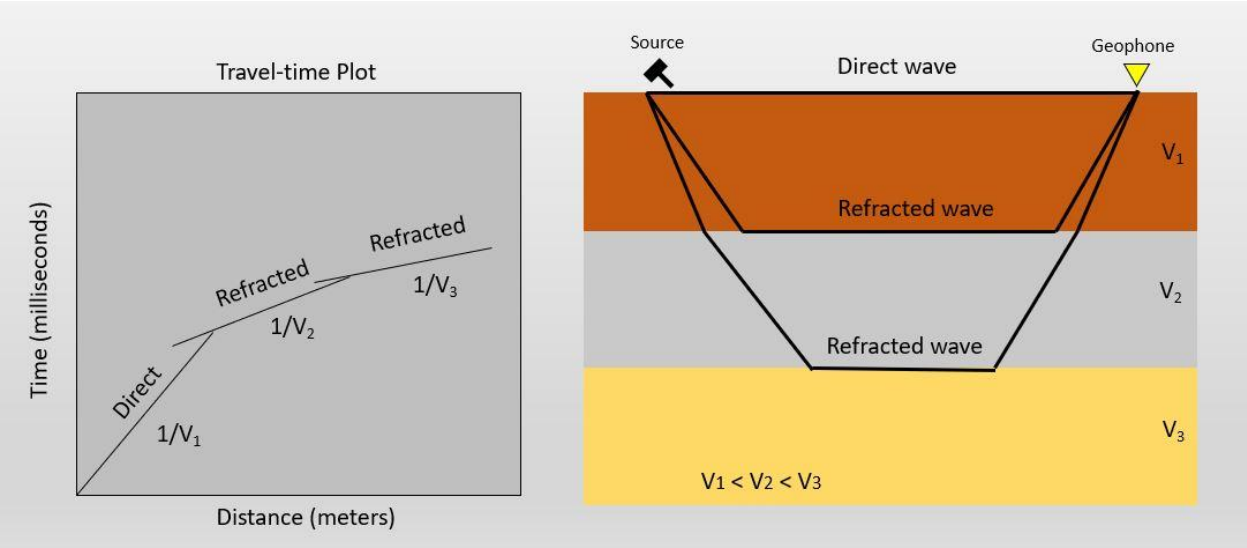

Figure 9**:** *Refracted waves travel more distance than the direct wave and therefore come in after the direct wave, assuming V3>V2>V1. Slopes of these refracted waves are shallower on the time travel plot, because they are traveling a longer distance in a shorter period of time. A trace of the refracted waves' slopes to the y-axis can be used to determine the depth of the interface(s) (Burger et al., 2006).*

This works because the travel time of the wave depends on the velocities of the wave in subsurface material. As P-waves emanate from a source, they are continually refracted upwards towards the surface because of the gradational increase in seismic velocity with depth (Shearer, 2009). (This is operating under the assumption that seismic velocity increases with depth, which is generally the case as incompressibility increases, except for anomalous low-velocity zones.) The head waves created by the waves' interactions with faster-velocity material travel faster than the direct wave, and they can arrive at the geophone faster than the direct wave, despite traveling a longer distance. Determining different slopes for lines to fit travel time curves can show the depth and velocity of subsurface layers (Figure 9).

Transdimensional Bayesian Inversion modeling

At this point in the project, the only data available are distances and the first arrival times of the P-waves. Without digging into the subsurface, there is no way to know what materials are present, in what quantities, and their distribution in three dimensions. Making use of Trans-dimensional Bayesian Inversion, a computer program can explore the given information and suggest possible 1-D models to explain the data (Charvin et al., 2009).

Inversion has been used since the early part of the twentieth century to produce models of subsurface velocity distributions from time-travel curves (Lowrie, 2007). Trans-dimensional Bayesian Inversion is a form of inversion that uses a Markov Chain Monte Carlo (MCMC) algorithm to suggest possible models to fit provided data. A Matlab program using the MCMC algorithm "randomly wanders"

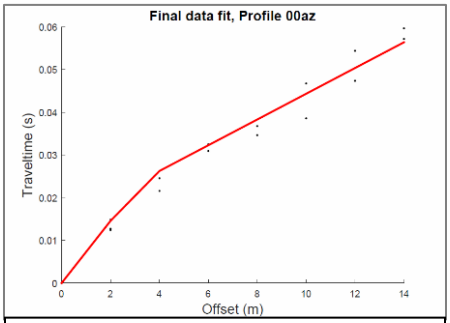

Figure 10: *Showing a possible best-fit curve for P-wave arrival times for the North-South azimuth of the 12m array. Different slopes indicate layers of different velocities. This particular model suggests the existence of three different layers, the deepest of which has a higher velocity than the other two, which have very similar slopes.*

around a field of time and distance, suggesting velocities, depths, and number of layers, trying to find a best-fit for the provided data (Figure 10). The word "trans-dimensional" indicates that the program is free to add or remove layers (Bodin and Sambridge, 2009), with fewer layers being preferred. By doing this, the program creates random models that are then compared against provided acceptance conditions and fit requirements. If the model does not conform to those conditions, it is discarded, and another model is attempted. Millions of iterations can be tested in the space of five minutes to close in on potential models. This method produces many possible 1-D models that satisfy the data given what little information is known. For the current project, one million iterations were run for each line of azimuth, of which two thousand were ultimately saved and recorded (Figure 11).

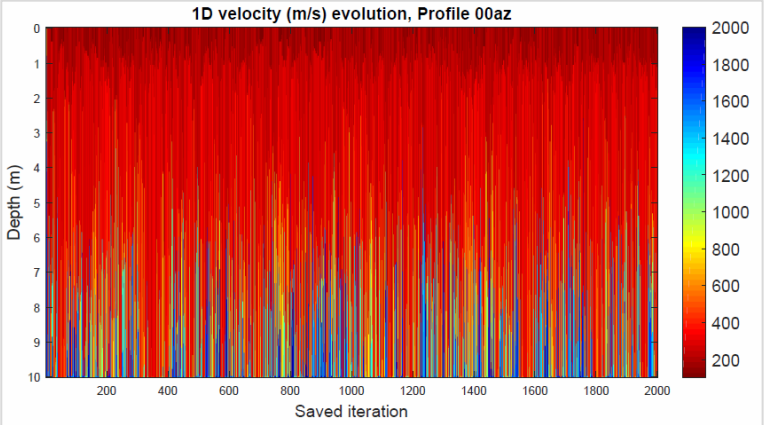

Figure 11: *Each vertical line represents one of 2000 potential models to fit the data for the North-South azimuth of the 12m array. Different colors indicate different suggested velocities (m/s) at different depths.*

Each run of the program produces the following figures: 1) a best fit line for points on the time-travel curve as seen above in Figure 10, 2) a histogram showing where models support the placement of a discontinuity, 3) a histogram showing the number of layers the models show may be in the system, 4) the probability density model, and 5) a 1-D model showing the average velocity with depth and error bars of all the models for the specified subset of data (Figure 12).

It is from this 1-D model that we can see how well constrained the models are. Below 4m, constraints on the velocities begin to weaken as the error gets larger and larger, so the model can be cut off at this depth. This is the depth resolution, and this means that the resolution is best to about 4m below the surface using the 12m array. This is consistent with the expected resolution returned from a linear array of comparable size (Burger et al., 2006))

Results

The velocities and errors associated with specific depths returned by the modeling are then graphed based on azimuthal direction. It is this relationship that would reveal patterns of anisotropy that can then be compared to regional and local trends. Figures 13 and 14 show these relationships. Unfortunately, few points in either array occur far enough away from the mean velocity to be considered significant. There is an overwhelming amount of error. In the absence of error, the patterns from the second locality could be considered interesting; there is a curve that is vaguely sinusoidal (Figure 14). The error cannot be dismissed so simply, however. Therefore, patterns of anisotropy cannot be discerned at this resolution for either of these arrays.

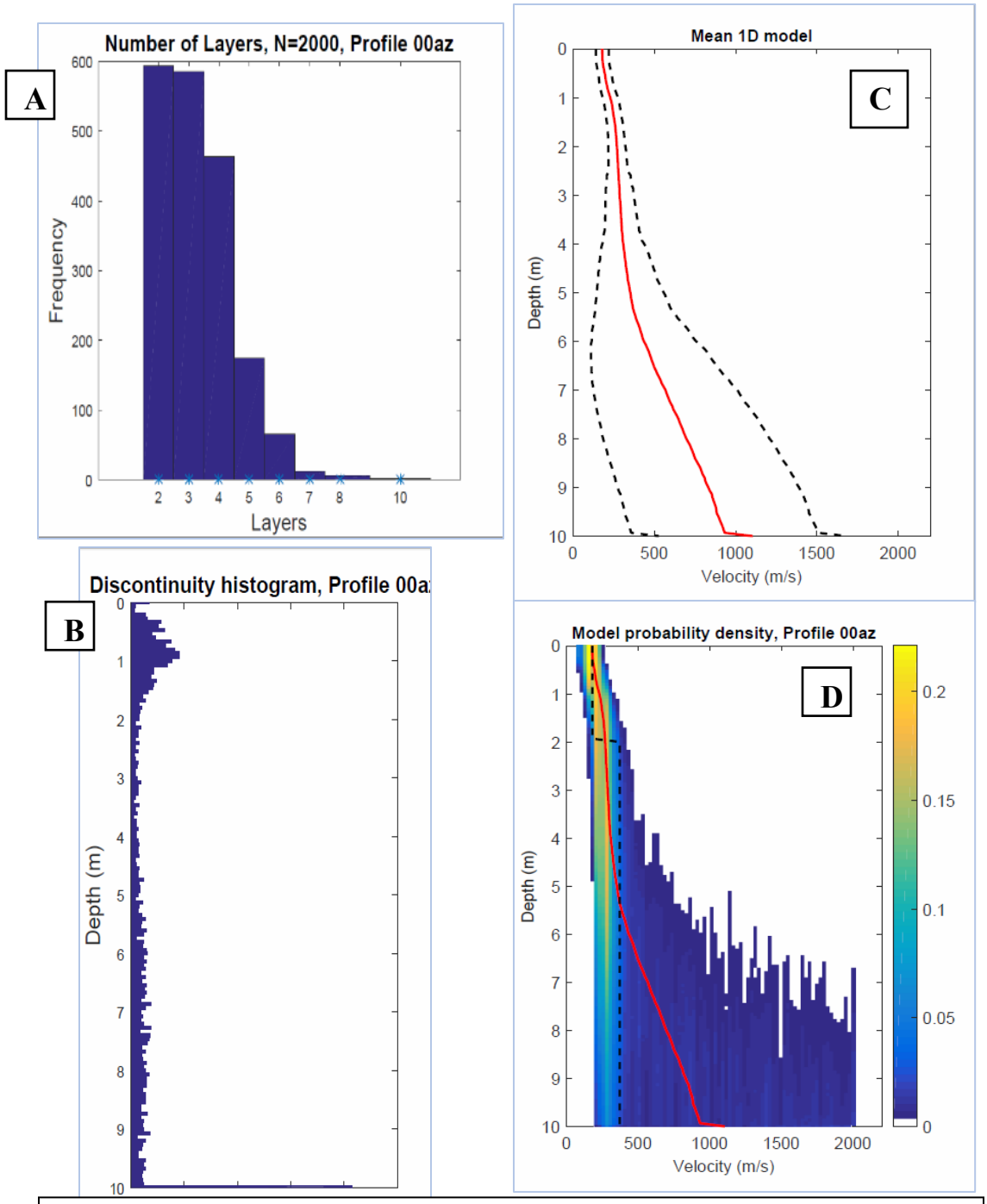

Figure 12: *Resulting figures from running Matlab program for North-South azimuth of the 12m array.*
A) *Histogram showing the frequency of the maximum number of layers suggested over the course of 2000 iterations. For this particular line of azimuth, most iterations support presence of two or three layers.*
B) *Histogram showing the frequency of suggestion of discontinuities (layer transitions) at certain depths for the selected line of azimuth*
C) *1D model of the average velocity (red) vs. depth of all 2000 saved iterations for the selected line of azimuth, with associated errors (dashed)*
D) *Probability density model, showing the mean velocity (red), likely position of discontinuities (dashed), and percentage of iterations that agreed on possible velocities (warmer color equals higher number of iterations in agreement).*

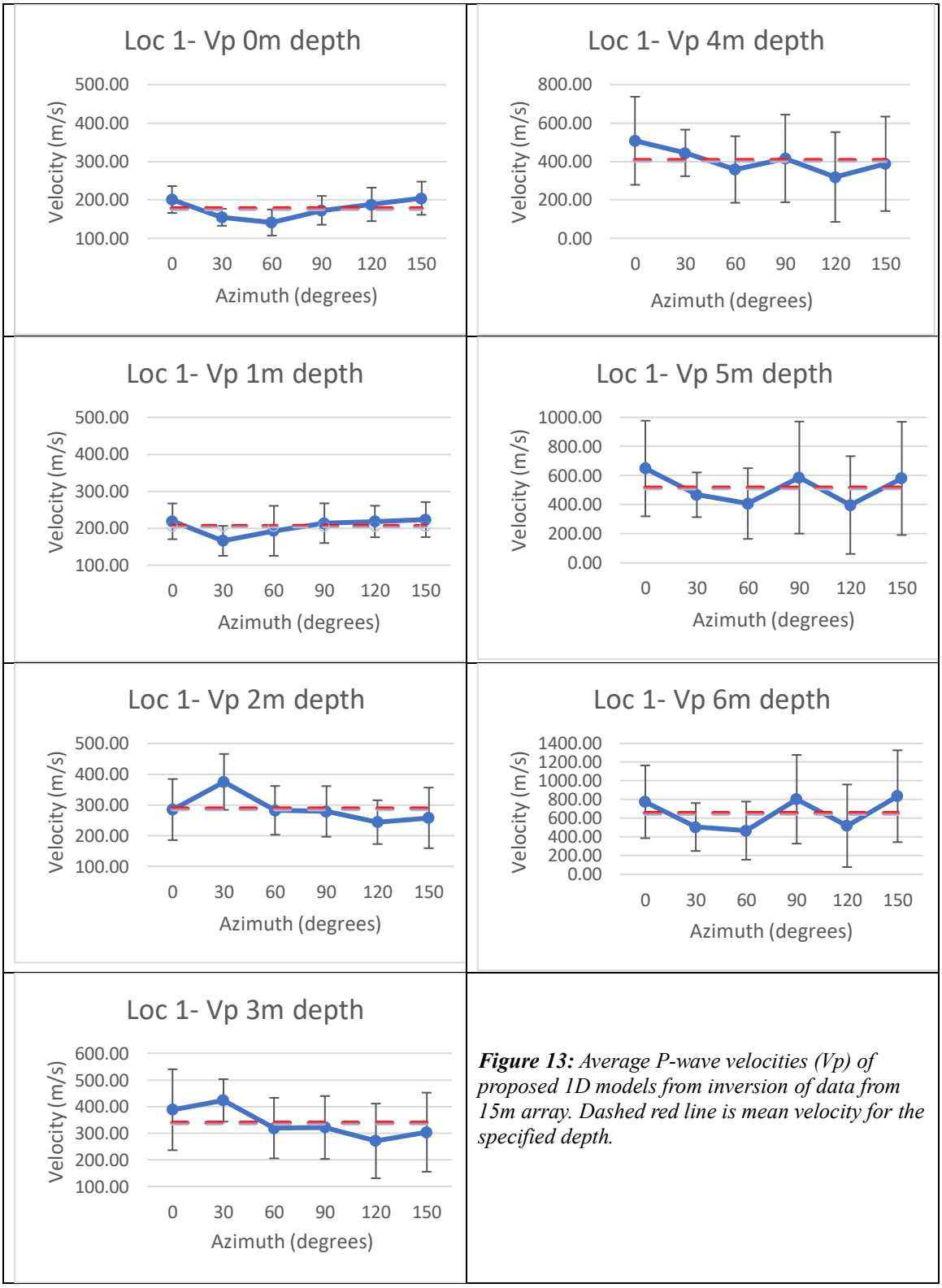

Figure 13: *Average P-wave velocities (Vp) of proposed 1D models from inversion of data from 15m array. Dashed red line is mean velocity for the specified depth.*

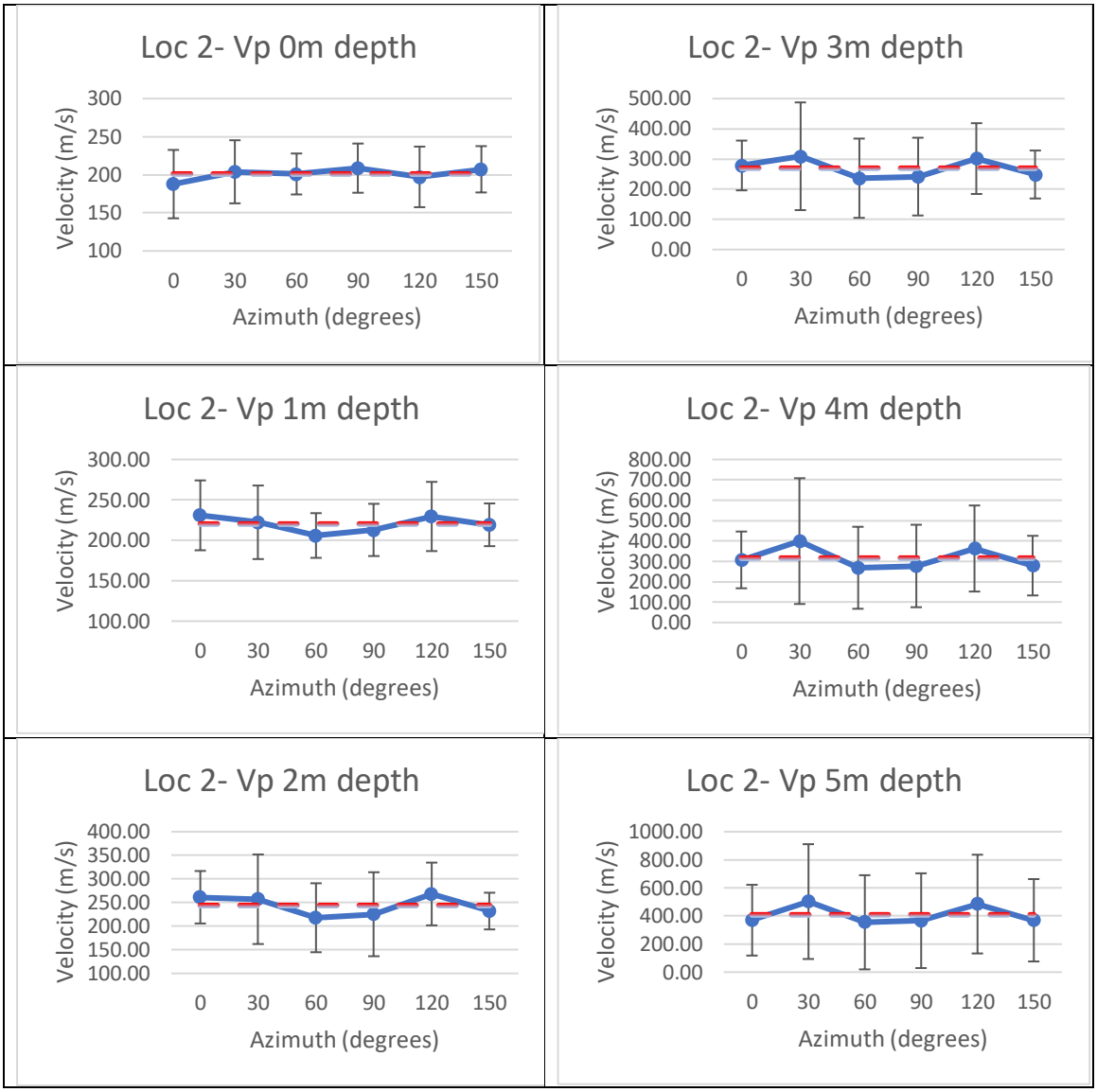

***Figure 14**: Average P-wave velocities (Vp) proposed by 1D models from inversion of data for 12m*

Discussion

Few conclusions can be made in the face of such high error. The resolution of the data does not allow for identification of anisotropy at its current ratio beneath these two locations. However, this project does allow us to put an upper bound on the amount of anisotropy present. The anisotropy must be less than the error associated with our modeled velocities. Otherwise, the patterns of anisotropy would be discernable despite the limited resolution. Table 1 lists the upper bounds on the percentage difference in velocities between slow and fast directions that could be detectable, with the project in its current form. For example, in the 15m circle, the amount of anisotropy present at a depth of 4 meters must be less than 51%, otherwise a pattern would be obvious despite the high error.

Table 1: Upper Bounds on Ratio of Anisotropy (Average Error/Average Velocity)*100%		
15m Array	**Depth**	**Upper Bound**
	0m	20%
	1m	24%
	2m	30%
	3m	37%
	4m	51%
	5m	59%
	6m	60%
12m Array	0m	18%
	1m	17%
	2m	29%
	3m	44%
	4m	64%
	5m	80%

Many factors could have affected the uncertainty of the data collected in the field, resulting in the large amount of error returned by the modeling. Extra time and care could have been taken to reduce error and increase resolution in the field. Unfortunately, these efforts were restricted by the finite amount of available time and space at the site. The arrays were not on perfectly flat ground; instead, the ground was rutted from the treads of construction-grade digging equipment. In some cases, geophones were inserted into a 0.5 m berm of unconsolidated sediments, which could add as much as 3ms to the associated travel times. Other geophones had to be inserted into soil where grasses and other plants were growing, the impact of which is currently unknown. Several shots for both arrays had to be omitted entirely because of the position of trees and topography in relation to the arrays. Issues like these affect the number and efficacy of data points and, by extension, the resolution of the model.

To increase resolution for this method, more data points are needed in general. More specifically, increasing the diameter of the array would increase the depth resolution, and allow the modeling to "see" deeper below the surface. A larger number of shots per line of azimuth would help reduce noise in the data up to the maximum resolvable depth that is allowed by the diameter of the array. Combining these would allow for better resolution at greater depths. This project could also be adapted by rotating a linear array around a central axis. This would increase the resolution in a similar way by increasing the number of sensors on each line of azimuth.

Use of this particular inversion method assumes the subsurface is more-or-less a horizontal "layer cake", meaning the dips of any layers are negligible and the subsurface can be represented as a one-dimensional model. This may not be a safe assumption. As mentioned previously, this region has experienced significant deformation in the past, but to explore this possibility further would require use of a two-dimensional model (which I am led to believe is somewhat beyond the scope of an undergraduate thesis).

Conclusion

To summarize, I have not found strong signs of anisotropy using this method, but I can place an upper bound on the amount of anisotropy present at these two locations. Recommendations for future efforts include increasing the amount of cleared land available to allow for larger-diameter arrays, increasing the number of shots or sensors per line of azimuth, and evaluation for the necessity of two-dimensional modeling. Due to the enormous amount of error returned from the modeling, the experiment in its current state cannot conclusively indicate

where Mr. Jacobsen should focus his digging efforts. The resolution of the project supports the NULL hypothesis. However, with modification, this experiment does show potential for identifying anisotropy that could be associated with veins.

Acknowledgements

The author would like to extend thanks to Ed Jacobsen, for allowing use of his property for this project. Rebecca Butcher, Kelsey Wood, Joe Schools, Angela Marusiak, and Ross Maguire helped collect data in the field. Further thanks go to Clifford Lindsay and Sarah Householder for manuscript comments and editing, and to Eleanor Russell for help with the figures.

Bibiliography

Campbell, Ian. (1927). Alpine mineral deposits. *American Mineralogist* v. 12, pp. 157-167. <http://www.minsocam.org/msa/collectors_corner/arc/alpine.htm.> Accessed 4/12/2018

Brown, D.L. and Wilson, W.E. (2001). The Rist and Ellis Tracts, Hiddenite, North Carolina. *Mineralogical Record, 32(2),* 129-139.

Bodin, T., and Sambridge, M. (2009). Seismic tomography with the reversible jump algorithm. *Geophys. J. Int.* 178, 1411–1436. doi: 10.1111/j.1365-246X.2009.04226.x

Burger, R.H., Sheehan, A.F., & Jones, C.H. (2006). *Introduction to applied geophysics: Exploring the shallow subsurface*. New York: W.W. Norton.

Charvin, K., Gallagher, K., Hampson, G., & Labourdette, R., (2009). A Bayesian approach to inverse modelling of stratigraphy, part 1: method, *Basin Research*, 21(1), 5–25.

Cheraghi, S., Craven, J.A., & Bellefleur, G., 2015, Feasibility of virtual source reflection seismology using interferometry for mineral exploration: A test study in the Lalor Lake volcanogenic massive sulphide mining area, Manitoba, Canada. *Geophysical Prospecting*, 63, 833-848. DOI: 10.1111/1365-2478.12244

Crampin, S. (1981). A review of wave motion in anisotropic and cracked elastic-media, *Wave motion*, 3(4), 343-391, doi:10.1016/0165-2125(81)90026-3.

Drake, A.A., Jr., Sinha, A.K., Laird, J., and Guy, R.E. (1989) *The Taconic orogeny* in Hatcher, R.D., Jr., Thomas, W.A., and Viele, G.W., eds., The Appalachian-Ouachita orogeny in the United States: Boulder, Colorado, Geological Society of America, Geology of North America, v. F-2, p. 101-177.

Hatcher, R. D., Jr., Osberg, P.H., Drake, A.D., Jr., Robinson, P., and Thomas, W.A. (1990). *Tectonic map of the U.S. Appalachians in The Appalachian-Ouachita Orogen in the United States*: Boulder, Colorado, Geological Society of America, Geology of North America, v. F-2, Plate 1.

Lowrie, W. (2007). *Fundamentals of Geophysics*. Cambridge: Cambridge University Press. DOI: 10.1017/CBO9780511807107

Novitsky, C.G., Holbrook, W.S., Carr, B.J., Pasquet, S., Okaya, D., & Flinchum, B.A. (2018) Mapping inherited fractures in the critical zone using seismic anisotropy from circular surveys. *Geophyiscal Research Letters* (2018) DOI: 10.1002/2017GL075976

Palache, C., Davidson, S.C., and Goranson, E.A. (1930). The Hiddenite Deposit in Alexander County, North Carolina; *American Mineralogist*, v. 15, no. 8, p. 280-302.

Rankin, D.W., Drake, A.A., Jr., Glover, L., III, Goldsmith, R., Hall, L.M., Murray, D.P., Ratcliffe, N.M., Read, J.F., Secor, D.T., Jr., and Stanley, R.S. (1989) *Pre-orogenic terranes* in Hatcher, R.D., Jr., Thomas, W.A., and Viele, G.W., eds., The Appalachian-Ouchita orogeny in the United States: Boulder, Colorado, Geological Society of America, Geology of North America, v. F-2, p. 7-100.

Shearer, P. M. (2009). *Introduction to Seismology*. Cambridge: Cambridge University Press.

Sinkankas, J. (1976): *Gemstones of North America* **2**. Van Nostrand Reinhold, New York, N.Y. (18-32, 78).

Sinkankas, J. (1989). *Emeralds and Other Beryls*. Prescott, AZ: Geoscience Press.

Speer, W.E., 2008, *Emerald Crystal Pockets of the Hiddenite District, Alexander County, North Carolina, Fieldtrip Guidebook*, Geological Society of America, Southeastern Section 57th Annual Meeting April 2008, Charlotte, North Carolina, USA

Stephan, R. A. (1985). *Seismic anisotropy in the upper oceanic crust*, Journal of Geophysical Research., 90, 11,383–311,396.

Tacker, C.R. (1999): Preliminary observations of the emerald deposits of Hiddenite, North Carolina, USA. *Geol. Soc. Am., Abstr Program*s **31**, 306.

Tsuji, T., et al. (2011). In situ stress state from walkaround VSP anisotropy in the Kumano basin southeast of the Kii Peninsula, Japan, *Geochemistry Geophysics Geosystems*, *12*, 10.1029/2011gc003583.

Wise, M.A. (2008). Mineralogy of the Gem-Bearing Alpine-Type Quartz Veins from Hiddenite, North Carolina; abstract, 29th Annual FM-MSA-TGMS Tucson Mineralogical Symposium, Classic Mineral Localities of the United States*, Mineralogical Record*, v. 39 Jan-Feb, p. 56. Presented by Wise Feb 16, 2008 at the Tucson Gem and Mineral Show, Tucson, Arizona.

Wise, M.A., and Anderson, A.J. (2006). The Emerald- and Spodumene-Bearing Quartz Veins of the Rist Emerald Mine, Hiddenite, North Carolina: *The Canadian Mineralogist*, v. 44, p. 1529-1541.

Appendix

Probability density models – 15m Array

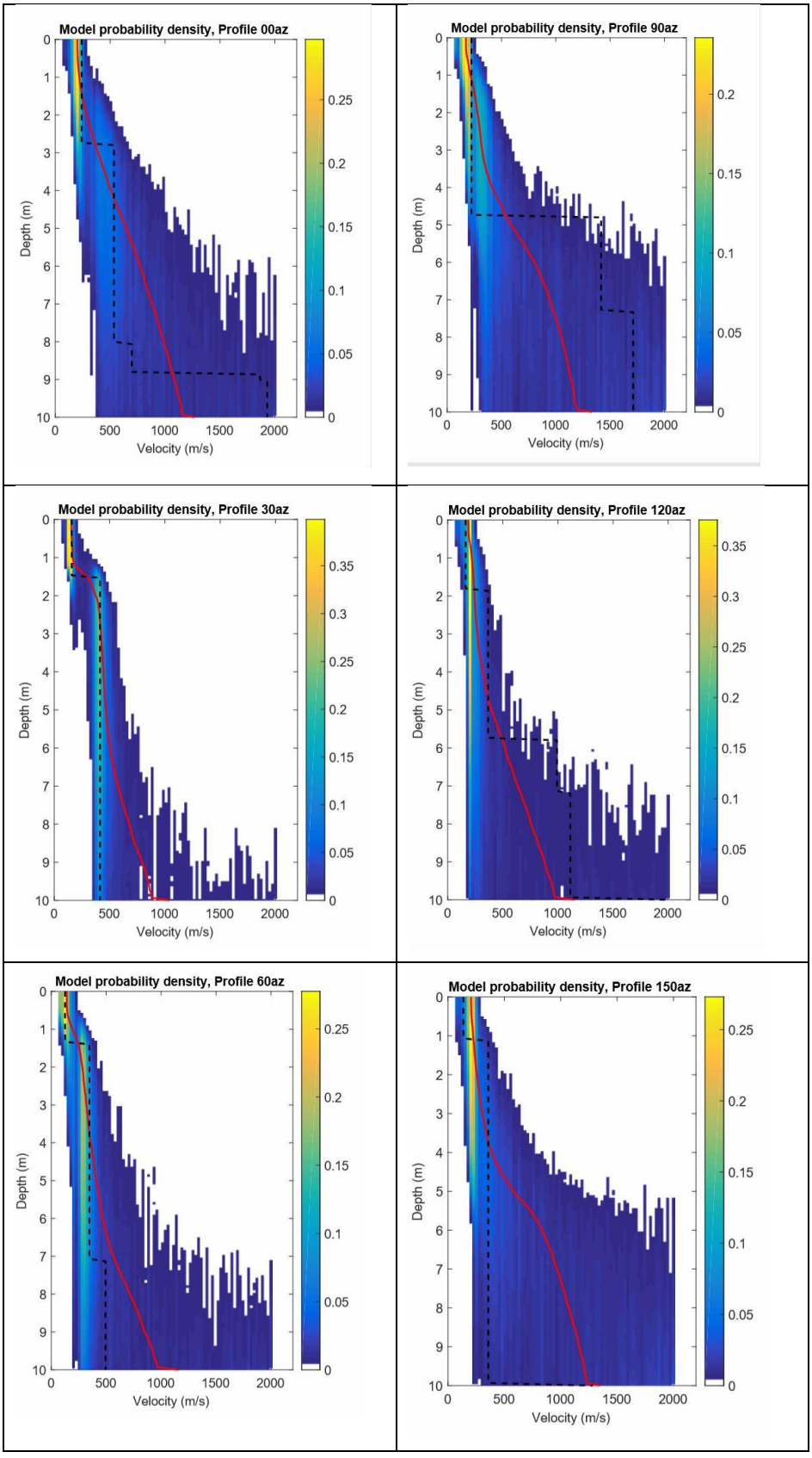

Probability density models – 12m Array